

Hydrological change in Southern Europe responding to increasing North Atlantic overturning during Greenland Stadial 1

Miguel Bartolomé^{a,b,1}, Ana Moreno^{a,c}, Carlos Sancho^b, Heather M. Stoll^d, Isabel Cacho^e, Christoph Spötl^f, Ánchel Belmonte^b, R. Lawrence Edwards^g, Hai Cheng^{g,h}, and John C. Hellstromⁱ

^aInstituto Pirenaico de Ecología, Consejo Superior de Investigaciones Científicas, 50059 Zaragoza, Spain; ^bDepartamento de Ciencias de la Tierra, Universidad de Zaragoza, 50009 Zaragoza, Spain; ^cLaboratorio Internacional de Cambio Global, Pontificia Universidad Católica de Chile, Consejo Superior de Investigaciones Científicas, 8331150 Santiago, Chile; ^dDepartamento de Geología, Universidad de Oviedo, 33005 Oviedo, Spain; ^eDepartament d'Estratigrafia, Paleontologia i Geociències Marines, Universitat de Barcelona, 28080 Barcelona, Spain; ^fInstitut für Geologie, Universität Innsbruck, 6020 Innsbruck, Austria; ^gDepartment of Earth Sciences, University of Minnesota, Minneapolis, MN 55455; ^hInstitute of Global Environmental Change, Xian Jiaotong University, Xian 710049, China; and ⁱSchool of Earth Sciences, University of Melbourne, Melbourne, VIC 3010, Australia

Edited by Mark H. Thiemens, University of California, San Diego, La Jolla, CA, and approved April 14, 2015 (received for review February 26, 2015)

Greenland Stadial 1 (GS-1) was the last of a long series of severe cooling episodes in the Northern Hemisphere during the last glacial period. Numerous North Atlantic and European records reveal the intense environmental impact of that stadial, whose origin is attributed to an intense weakening of the Atlantic Meridional Overturning Circulation in response to freshening of the North Atlantic. Recent high-resolution studies of European lakes revealed a mid-GS-1 transition in the climatic regimes. The geographical extension of such atmospheric changes and their potential coupling with ocean dynamics still remains unclear. Here we use a subdecadally resolved stalagmite record from the Northern Iberian Peninsula to further investigate the timing and forcing of this transition. A solid interpretation of the environmental changes detected in this new, accurately dated, stalagmite record is based on a parallel cave monitoring exercise. This record reveals a gradual transition from dry to wet conditions starting at 12,500 y before 2000 A.D. in parallel to a progressive warming of the subtropical Atlantic Ocean. The observed atmospheric changes are proposed to be led by a progressive resumption of the North Atlantic convection and highlight the complex regional signature of GS-1, very distinctive from previous stadial events.

speleothem | Iberia | Younger Dryas | stable isotopes | Greenland Stadial 1

The last deglacial warming was interrupted by a rapid cooling identified in Greenland ice cores as Greenland Stadial 1 (GS-1) at 12,846 y before 2000 A.D. [b2k, Greenland ice core chronology 2005 (GICC05)] (1), previously defined as Younger Dryas (YD) based on vegetation changes recorded in Europe (2). Although the forcing mechanism for this climate change is still under discussion (3), the most plausible trigger is related to catastrophic freshwater release into the North Atlantic and the consequent reduction in the Atlantic Meridional Overturning Circulation (AMOC) (4). Recently published high-resolution North European terrestrial records indicate two phases within GS-1, with the second phase characterized by rapid alternations between glacier advances and retreats (Lake Kråkenes, Norway) (5) and interpreted as a climatic amelioration based on an increase in detrital content and lamina thickness (Meerfelder Maar lake, Germany) (6) (Fig. 1). Records from the Atlantic Ocean, although of limited sampling resolution and not so well-constrained chronology, also indicate internal variability during GS-1, expressed as changes in sea surface salinity, temperature, and sea ice extension in parallel to modifications in the intensity and location of the North Atlantic deep overturning cells (5, 7–9) (Fig. 1). These marine sequences reveal rapid shifts between weak and strong modes of deep convection during the last deglaciation with potential consequences for European environments that need to be further assessed. The Northern Iberian Peninsula (IP), located within the polar front during the time of the coldest temperatures in GS-1

(10), is a very sensitive location to determine the exact sequence of temperature and hydrological changes in Southern Europe during this stadial, not yet well resolved due to the lack of high-resolution records (11–13). Here, we present the first stalagmite record, to our knowledge, that covers the entire GS-1 period in Southern Europe, providing an excellent and independent chronological framework and a high-resolution climate reconstruction of this event, allowing understanding of the climate mechanisms that caused the mid-GS-1 transition.

Seso Cave System (42°27'23.08"N, 0°02'23.18"E, 794 m above sea level; Fig. 1) in the Central Pyrenees provides an unusually direct record of temperature and moisture balance during GS-1 because the climate proxies in stalagmites can be directly calibrated to the instrumental record in actively growing modern stalagmites (see *Supporting Information*). Speleothem formation occurred during short intervals since 40 ka, and became more widespread during the Holocene. Today, the modern climatology of moderate rainfall (mean annual precipitation is 900 mm, concentrated in spring and fall) and mild temperatures (mean annual *ca.* 13 °C), together with a vegetation cover dominated by *Pinus sylvestris* and *Quercus ilex*, fuel speleothem growth. We present the record of SE09-6, a 160-mm-long stalagmite obtained in situ from the inner part of the cave where the temperature is constant throughout the

Significance

This study presents robust evidence of two hydrological phases within the Greenland Stadial 1 (GS-1) cold event (12.8–11.7 ka B.P.) in Southern Europe. We present a well-dated high-resolution speleothem record (Seso Cave, Central Pyrenees) where temperature and hydrological signals are independently reconstructed. Detailed interpretation of stable isotopes and trace elements allow characterizing a first dry period followed, after 12,500 y before 2000 A.D., by more humid conditions. Our findings point to the resumption of the Atlantic overturning circulation as the main mechanism behind the hydrological response in Europe during this mid-GS-1 transition. The second phase, cold in Greenland but humid in Western Europe, represents a new paradigm in the well-established model of dry, cold stadials during the last glacial period.

Author contributions: M.B., A.M., and C. Sancho designed research; M.B., A.M., C. Sancho, and Á.B. performed research; H.M.S., I.C., C. Spötl, R.L.E., H.C., and J.C.H. contributed new reagents/analytic tools; M.B., H.M.S., I.C., C. Spötl, Á.B., R.L.E., H.C., and J.C.H. analyzed data; and M.B., A.M., C. Sancho, H.M.S., I.C., C. Spötl, Á.B., R.L.E., H.C., and J.C.H. wrote the paper.

The authors declare no conflict of interest.

This article is a PNAS Direct Submission.

¹To whom correspondence should be addressed. Email: mbart@ipe.csic.es.

This article contains supporting information online at www.pnas.org/lookup/suppl/doi:10.1073/pnas.1503990112/-DCSupplemental.

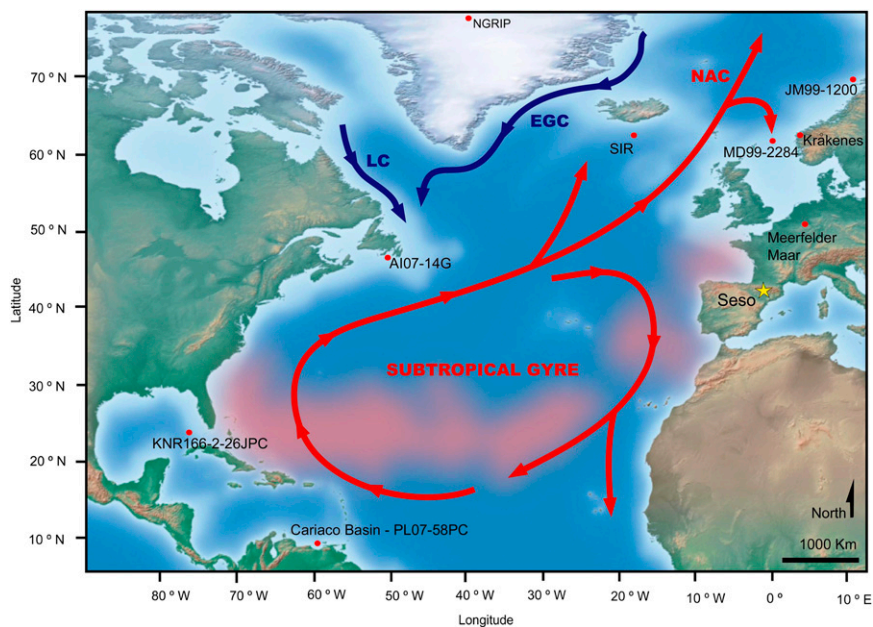


Fig. 1. Schematic map showing North Atlantic surface circulation with location of selected records. Geographic situation of the studied record from Seso Cave System (Central Pyrenees, Spain) together with European lake sequences [Meerfelder Maar (6) and Kråkenes (5)] and several marine cores cited in the text [PL07-58PC from Cariaco Basin (24), KNR166-2-26JPC from Florida Straits (21), AI07-14G from Newfoundland (9), multiple cores from South Iceland Rise (SIR) (23), MD99-2284 from the Faeroe-Shetland passage (5), and JM99-1200 off Northern Norway (7)]. Pinkish area marks the source of modern moisture to the IP (22). EGC, East Greenland Current; LC, Labrador Current; NAC, North Atlantic Current.

year (11.7 °C). The age model is based on 17 U/Th dates ranging from $12,958 \pm 52$ – $11,672 \pm 68$ y b2k (Dataset S1 and SI Appendix, Figs. S1 and S2), thus covering the GS-1 as defined in North Greenland ice core project (NGRIP) (GICC05) (1). The 1-mm proxy analyses therefore represent an average sampling resolution of 8.6 y.

Results and Discussion

Two Hydrological Scenarios Within GS-1. SE09-6 speleothem $\delta^{13}\text{C}$ and Mg/Ca data point to two distinct phases with a gradual transition in between (Fig. 2). The $\delta^{13}\text{C}$ and Mg/Ca show higher values between 12,920 y b2k and 12,500 y b2k, a gradual decrease until ca. 12,000 y b2k, and a phase with lower values until the Holocene onset at 11,700 y b2k. Monitoring of Seso Cave shows low speleothem $\delta^{13}\text{C}$ and Mg/Ca values coinciding with increased infiltration into the cave as a result of a higher precipitation–evaporation balance in the region (SI Appendix, Fig. S3). This is consistent with well-documented processes by which slower drip rates enhance degassing and raise dripwater Mg/Ca ratios and $\delta^{13}\text{C}$ values (14). In $\delta^{13}\text{C}$, this trend can be amplified when higher humidity increases soil CO_2 production and reduces atmospheric dilution, conserving lower soil $\delta^{13}\text{C}$. Very stable $\delta^{234}\text{U}$ values in this stalagmite (SI Appendix, Fig. S4) are suggestive of constant rock–water interaction processes (15). Consequently, we interpret $\delta^{13}\text{C}$ as a humidity proxy. Therefore, the $\delta^{13}\text{C}$ record suggests a first phase of relatively drier conditions until 12,500 y b2k and a progressive increase in humidity afterward. On the other hand, prior calcite precipitation (PCP), and thereby the Mg/Ca ratio, are enhanced by slower drip rates, and also by higher dripwater saturation states. These combined effects can be disentangled by comparing Mg/Ca to a second factor responsive to dripwater saturation state and drip interval, such as the stalagmite growth rate. Growth rates in SE09-6 vary from 0.04 mm/y to 0.13 mm/y throughout the YD with a marked increase after 12,500 y b2k (SI Appendix, Fig. S5). Application of stalagmite growth rate and PCP using kinetics of Dreybrodt (16), in the I-STAL model (17), allows us to derive an inverse solution of variation in drip rate (drip interval) and dripwater saturation state that could produce the observed variations in Mg/Ca and stalagmite

growth rate constrained by the U/Th chronology. The modeled drip rates therefore indicate a shift to slightly drier conditions at the onset of GS-1 that lasted until about 12,000 y b2k (SI Appendix, Fig. S5). After 12,000 y b2k, the late YD is characterized by strongly increasing water availability represented by lower Mg/Ca values, which is consistent with the $\delta^{13}\text{C}$ data (Fig. 2).

Interpreting $\delta^{18}\text{O}$ Signal in Seso Cave. In contrast to the humidity proxies, $\delta^{18}\text{O}$ does not show such a two-phase evolution during GS-1. The $\delta^{18}\text{O}$ values decrease by 2.1‰ between 12,920 y b2k and 12,700 y b2k (Fig. 2), which is similar to the only published $\delta^{18}\text{O}$ data from a European stalagmite covering the same period (18). The $\delta^{18}\text{O}$ remains low up to 11,750 y b2k and then increases rapidly until onset of the Holocene. Although this pattern is similar to the NGRIP $\delta^{18}\text{O}$ record (GICC05), this similarity reduces after 12,500 y b2k when the NGRIP record slightly tends toward higher values, while the SE09-6 speleothem does not follow that pattern and remains stable (Fig. 2). Analysis of oxygen isotopes in a modern stalagmite from Seso suggests a strong dependence on air temperature through its influence on rainfall $\delta^{18}\text{O}$, providing a reliable proxy for the temperature evolution during GS-1 (Supporting Information). Thus, based on the correlation among recent speleothem $\delta^{18}\text{O}$ data and several instrumental temperature records and reconstructions (SI Appendix, Figs. S7 and S8), the $\delta^{18}\text{O}$ variation in SE09-6 of 2.14‰ during GS-1 is calculated to represent a 1.3 °C drop of the annual temperature. This estimate is subject to uncertainties due to possible $\delta^{18}\text{O}$ changes in the source area (ice volume, fresh water pulses, etc.) and the amount effect. The amount effect on the speleothem $\delta^{18}\text{O}$ in this cave is evident in a 3-y monitoring survey, whereby $\delta^{18}\text{O}$ of calcite measured on glass slides show higher values during drier winters, attenuating the $\delta^{18}\text{O}$ amplitude range and thus partially cancelling the temperature effect (SI Appendix, Fig. S9). In fact, during the second phase of GS-1 characterized by an increase in humidity, we expect a dominant influence of the amount effect (more negative $\delta^{18}\text{O}$ values) that would compensate the postulated increase in temperature (less negative $\delta^{18}\text{O}$ values). Coherently, the correlation between $\delta^{18}\text{O}$

along the GS-1 probably due to its high-latitude position, well within the zone of polar air masses.

Terrestrial records from North Europe also indicate the occurrence of some intra-GS-1 transition supporting our hypothesis (Fig. 3). An abrupt change is first detected in Meerfelder Maar (North Germany) at $12,240 \pm 40$ varve years proposed to reflect a climate amelioration led by a northward shift of the westerlies (6), which would be consistent with the northern location of the polar front indicated by the marine records. Farther north, the Kråkenes (South Norway) Ti record also supports two phases within GS-1, with an abrupt transition occurring slightly later, at 12,150 y b2k (Fig. 3). This change has been related to an increase in annual to decadal scale meltwater release from the nearby glacier, coincident with the incursion of warm waters into the Nordic Sea (5). This situation would lead to enhanced variability by the alternation of warm influx and meltwater fluxes, an instability also recorded in brine formation episodes in sediment cores south of Iceland (23). In such a context, Seso Cave represents the southernmost location where this mid-GS-1 transition is observed, and, coherently, it occurs before influencing northern records. In fact, this time-transgressive transition that occurred in Seso Cave at 12,500 b2k took about 350 y to migrate northward over more than 20 degrees of latitude. This intrastadial evolution in climate conditions over South Europe is further supported by recent Mediterranean marine records that detect warmer conditions by the second half of GS-1 (11), coherent with our hypothesis of a tight ocean–atmosphere coupling at this time-transgressive transition.

The enhanced humid conditions detected in our new Seso record after 12,500 y b2k, while temperatures were still low in Greenland, contrasts with the previous inference of uniformly cold, dry glacial stadials over Iberia (25). These findings would indicate that cold dry stadial conditions during GS-1 would have lasted for only a few centuries (12,900–12,500 y b2k) previous to a long transition to interstadial conditions. Further examination at high resolution of other glacial stadials will be needed to distinguish if these are also multiphase, or if GS-1 represents a distinctive type of stadial response observed during the deglaciation, and potentially transitional to the type of perturbations observed in the Holocene in Southern Europe (26). Future work on atmospheric mechanism will be required to resolve why the mid-GS-1 oceanic reorganization mostly affected regions located southward of polar air masses, with little variation recorded in Greenland.

Conclusion

The analysis of SE09-6 stalagmite from Seso Cave (Central Pyrenees) provides robust evidence of the existence of two different phases in GS-1 in terms of the hydrological response of terrestrial environments. The first phase, characterized by high values of $\delta^{13}\text{C}$ and Mg/Ca together with slow growth rates, is interpreted as a dry period with decreased infiltration into the cave resulting from lower precipitation–evaporation balance in the region. The chronological model based on 17 U/Th dates indicates the transition to a more humid period took place gradually, starting at 12,500 y b2k, well ahead of other terrestrial sequences in Northern Europe, such as Meerfelder Maar and Kråkenes Lake. This time-transgressive transition took about 350 y

from its record in Seso Cave to influence Northern European regions. Overall, there is a good correlation between the NGRIP temperature record and the $\delta^{18}\text{O}$ profile from Seso stalagmite that, supported by recent stalagmites from the same cave that overlap with the instrumental period, allows the extraction of a temperature signal. However, competing influences of the amount effect and temperature variation in the $\delta^{18}\text{O}$ signal controlled the second phase of GS-1, characterized by humid conditions while there were still cold atmospheric temperatures. This phase demands a new model for the well-established, archetypical, dry, cold stadials of the last glacial period. After comparison with marine sequences from the Atlantic Ocean, we conclude that the resumption of the Atlantic overturning circulation is the main mechanism behind the hydrological response in Europe during this mid-GS-1 transition. Therefore, a rapid coupling among terrestrial (atmospheric) and oceanic systems is evidenced at mid-GS-1 transition at a European scale.

Methods

Samples for isotopic ($\delta^{18}\text{O}$, $\delta^{13}\text{C}$) and trace element analyses were microdrilled at 1-mm resolution along the growth axis (SI Appendix, Fig. S1 and Dataset S1). One part of the isotopic analyses was performed at the University of Barcelona using a Finnigan-MAT 252 mass spectrometer, linked to a Kiel Carbonate Device III, with a reproducibility of 0.02‰ for $\delta^{13}\text{C}$ and 0.06‰ for $\delta^{18}\text{O}$. A second part of the samples was analyzed at the University of Innsbruck using a ThermoFisher DeltaPlusXL isotope ratio mass spectrometer coupled to a ThermoFisher Gas-Bench II. The long-term precision of the $\delta^{18}\text{O}$ and $\delta^{13}\text{C}$ values is 0.08 and 0.06‰ (1 sigma), respectively. In both laboratories, the results are reported relative to the Vienna Pee Dee Belemnite (VPDB) standard. Five Hendy tests were performed and showed no correlation between $\delta^{18}\text{O}$ and $\delta^{13}\text{C}$ (SI Appendix, Fig. S5). Trace elements were analyzed at the University of Oviedo using a Thermo inductively coupled plasma optical emission spectrometer. Samples were dissolved in 1.5 mL of dilute nitric acid (Tracepur) immediately before analysis and were introduced with a microflow nebulizer (0.2 mL/min), which permitted two replicate analyses. Mg was measured at 280.3 nm, in axial mode. Calibration was performed offline using the intensity ratio method (27).

A total of 17 U/Th ages were analyzed at the University of Minnesota (SI Appendix, Table S1) and at the University of Melbourne (SI Appendix, Table S1) following standard procedures (28). The calcite powder (150–200 mg) was dissolved in nitric acid, a mixed $^{229}\text{Th}/^{233}\text{U}/^{236}\text{U}$ tracer was added, and the sample was dried. After the addition of an iron chloride solution, NH_4OH was added drop by drop until the iron precipitated. The sample was then centrifuged to separate the iron from the rest of the solution, and the overlying liquid was removed. After loading the sample into columns containing anion resin, HCl was added to elute thorium and water was added to elute uranium. With the uranium and thorium separated, each sample was dried down, and dilute nitric acid was added. Analyses were conducted using a multicollector inductively coupled plasma mass spectrometer (Neptune Thermo Finnigan) and final ages are given as years before 2000 A.D. (b2k). The depth–age model was calculated with R (version 3.0.2) (29) using StalAge (30) (SI Appendix, Fig. S2). A reduction in the growth rate occurred at 120–110 mm (distance from the base), but no evidence of hiatus was observed in thin sections.

ACKNOWLEDGMENTS. We thank the editor and two anonymous reviewers for several insightful comments that significantly improved the paper. This is a contribution to HIDROPAST (CGL2010-16376), CGL2009-10455/BTE, and CUEVAS PPNN (258/2011) projects funded by the Spanish Ministry of Economy and Competitiveness, the European Regional Development Fund, and the National Parks Autonomous Organism. The integrating ice core, marine and terrestrial records (INTIMATE) Cost Action (Cost-ES0907) is acknowledged for funding a research stay by M.B. at Innsbruck University.

- Rasmussen SO, et al. (2006) A new Greenland ice core chronology for the last glacial termination. *J Geophys Res* 111:D06102.
- Mangerud J, Andersen ST, Berglund BE, Donner JJ (1974) Quaternary stratigraphy of Norden, a proposal for terminology and classification. *Boreas* 3(3):109–126.
- Meltzer DJ, Holliday VT, Cannon MD, Miller DS (2014) Chronological evidence fails to support claim of an isochronous widespread layer of cosmic impact indicators dated to 12,800 years ago. *Proc Natl Acad Sci USA* 111(21):E2162–E2171.
- Broecker WS (2006) Geology. Was the Younger Dryas triggered by a flood? *Science* 312(5777):1146–1148.
- Bakke J, et al. (2009) Rapid oceanic and atmospheric changes during the Younger Dryas cold period. *Nat Geosci* 2(3):202–205.
- Lane CS, Brauer A, Blockley SPE, Dulski P (2013) Volcanic ash reveals time-transgressive abrupt climate change during the Younger Dryas. *Geology* 41(12):1251–1254.
- Ebbesen H, Hald M (2004) Unstable Younger Dryas climate in the northeast North Atlantic. *Geology* 32(8):673–676.
- Thornalley DJR, Barker S, Broecker WS, Elderfield H, McCave IN (2011) The deglacial evolution of North Atlantic deep convection. *Science* 331(6014):202–205.
- Pearce C, et al. (2013) Ocean lead at the termination of the Younger Dryas cold spell. *Nat Commun* 4:1664.
- Broecker WS, et al. (1988) The chronology of the last Deglaciation: Implications to the cause of the Younger Dryas Event. *Paleoceanography* 3(1):1–19.
- Ausin B, et al. (2015) Coccolithophore productivity and surface water dynamics in the Alboran Sea during the last 25 kyr. *Palaeogeogr Palaeoclimatol Palaeoecol* 418:126–140.
- Morellón M, et al. (2009) Lateglacial and Holocene palaeohydrology in the western Mediterranean region: The Lake Estanya record (NE Spain). *Quat Sci Rev* 28(25–26):2582–2599.

Hydrological change in Southern Europe responding to increasing North Atlantic overturning during Greenland Stadial 1

by Miguel Bartolomé, Ana Moreno, Carlos Sancho, Heather Stoll, Isabel Cacho, Christoph Spötl, Ánchel Belmonte, R. Lawrence Edwards, Hai Cheng and John Hellstrom

1. Supplementary Methods

Seso Cave System (42°27'23.08''N; 0°02'23.18''E, 794 m a.s.l.; Fig.1) is a small, shallow and rectilinear pseudo-karstic system developed in a poorly soluble marly stratum between Eocene limestone beds. The cave's origin is related to piping processes that triggered mechanical scouring and outwashing mechanisms to evacuate the dispersive marly material (1). This study is focused on a 160 mm-long stalagmite (SE09-6) obtained in-situ from the inner part of the cave where temperature (11.7°C) and humidity (100%) are constant during the year. The stalagmite is cylindrical in shape and 50 mm in diameter with alternating columnar and microcrystalline calcite textures and showing mm-thin lamination (Fig. S1).

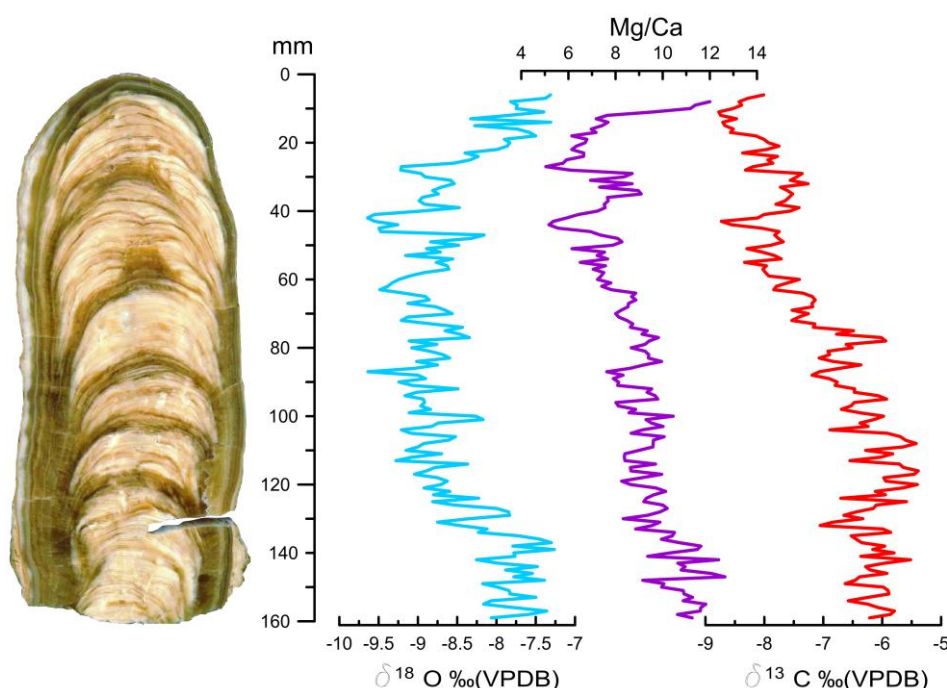


Figure S1. Slab of SE09-6 stalagmite showing variations of $\delta^{18}\text{O}$, $\delta^{13}\text{C}$ and Mg/Ca along the growth axis. VPDB(Vienna Pee Dee Belemnite)

The cave CO_2 values vary between ~501 to ~8570 ppm, with the lowest values during winter (more ventilation) and the highest in summer (less ventilation). In that part of the cave rock thickness is about 3 m and above there is a well-developed soil. The

stalagmite was not actively growing when collected (no drips or calcite precipitates). It was sampled every 1 mm along the growth axis and analyzed for stable isotopes ($\delta^{18}\text{O}$, $\delta^{13}\text{C}$) and trace elements (Mg/Ca) (Supplementary Data) (Fig. S1).

The age model is based on 17 U-Th dates ranging from $12,958 \pm 52$ to $11,672 \pm 68$ (Table S1, Fig S2) thus covering the GS-1 with an average sampling resolution of 8.6 years.

Table S1. ^{230}Th dating results (2σ errors). a, Ages from the University of Minnesota. b, Ages from the University of Melbourne. Activity ratios were determined using the decay previously published constants (2, 3)

a

^{230}Th dating results. The error is 2σ error.

Sample Number	^{238}U (ppb)	^{232}Th (ppt)	$^{230}\text{Th}/^{232}\text{Th}$ (atomic $\times 10^{-6}$)	$\delta^{234}\text{U}^*$ (measured)	$^{230}\text{Th}/^{238}\text{U}$ (activity)	^{230}Th Age (yr) (uncorrected)	^{230}Th Age (yr) (corrected)	$\delta^{234}\text{U}_{\text{initial}}^{**}$ (corrected)	^{230}Th Age (yr BP)*** (corrected)
Se-09-6-(155mm)	353.2 \pm 0.4	1044 \pm 21	924 \pm 19	457.0 \pm 1.7	0.1656 \pm 0.0003	13079 \pm 32	13021 \pm 52	474 \pm 2	12958 \pm 52
Se-09-6-(138mm)	325.2 \pm 0.4	949 \pm 19	935 \pm 19	457.8 \pm 1.7	0.1655 \pm 0.0004	13062 \pm 34	13005 \pm 53	475 \pm 2	12942 \pm 53
Se-09-6-(124mm)	336.4 \pm 0.5	1124 \pm 23	811 \pm 16	459.9 \pm 1.7	0.1643 \pm 0.0004	12940 \pm 36	12875 \pm 59	477 \pm 2	12812 \pm 59
Se-09-6-(110mm)	342.1 \pm 0.5	814 \pm 16	1122 \pm 23	477.8 \pm 1.7	0.1619 \pm 0.0004	12573 \pm 34	12527 \pm 47	495 \pm 2	12464 \pm 47
Se-09-6-(95mm)	356.0 \pm 0.6	853 \pm 17	1105 \pm 22	472.0 \pm 2.1	0.1605 \pm 0.0004	12518 \pm 36	12472 \pm 49	489 \pm 2	12409 \pm 49
Se-09-6-(80mm)	340.5 \pm 0.5	2221 \pm 45	401 \pm 8	464.9 \pm 1.9	0.1585 \pm 0.0004	12415 \pm 39	12287 \pm 99	481 \pm 2	12224 \pm 99
Se-09-6-(70mm)	350.0 \pm 0.6	2651 \pm 53	340 \pm 7	453.9 \pm 1.9	0.1563 \pm 0.0004	12335 \pm 39	12183 \pm 113	470 \pm 2	12120 \pm 113
Se-09-6-(55mm)	387.9 \pm 0.7	1931 \pm 39	510 \pm 10	460.1 \pm 1.9	0.1541 \pm 0.0004	12097 \pm 37	11999 \pm 78	476 \pm 2	11936 \pm 78
Se-09-6-(42mm)	332.0 \pm 0.6	1511 \pm 30	551 \pm 11	446.3 \pm 2.1	0.1520 \pm 0.0004	12042 \pm 40	11951 \pm 76	462 \pm 2	11888 \pm 76
Se-09-6-(30mm)	314.6 \pm 0.6	1351 \pm 27	573 \pm 12	438.9 \pm 2.3	0.1492 \pm 0.0004	11875 \pm 42	11789 \pm 74	454 \pm 2	11726 \pm 74
Se-09-6-(20mm)	313.3 \pm 0.6	1874 \pm 38	403 \pm 8	415.2 \pm 2.1	0.1461 \pm 0.0005	11820 \pm 43	11698 \pm 96	429 \pm 2	11635 \pm 96
Se-09-6-(7mm)	319.8 \pm 0.7	1166 \pm 23	672 \pm 14	441.2 \pm 2.4	0.1486 \pm 0.0005	11807 \pm 44	11735 \pm 68	456 \pm 3	11672 \pm 68

U decay constants: $\lambda_{238} = 1.55125 \times 10^{-10}$ (4) and $\lambda_{234} = 2.82206 \times 10^{-6}$ (5). Th decay constant: $\lambda_{230} = 9.1705 \times 10^{-6}$ (5). $^*\delta^{234}\text{U} = ([^{234}\text{U}/^{238}\text{U}]_{\text{activity}} - 1) \times 1000$. $^{**}\delta^{234}\text{U}_{\text{initial}}$ was calculated based on ^{230}Th age (T), i.e., $\delta^{234}\text{U}_{\text{initial}} = \delta^{234}\text{U}_{\text{measured}} \times e^{\lambda_{234} \times T}$. Corrected ^{230}Th ages assume the initial $^{230}\text{Th}/^{232}\text{Th}$ atomic ratio of $4.4 = 2.2 \times 10^{-6}$. Those are values for a material at secular equilibrium, with the bulk earth $^{232}\text{Th}/^{238}\text{U}$ of 3.8. The errors are arbitrarily assumed to be 50%. $^{***}\text{B.P}$ stands for “Before Present” where “Present” is defined as the year 1950 AD.

b

Sample (mm)	^{238}U (ppb)	$^{230}\text{Th}/^{238}\text{U}$ (activity)	$^{234}\text{U}/^{238}\text{U}$ (activity)	$^{232}\text{Th}/^{238}\text{U}$ (activity)	$^{230}\text{Th}/^{232}\text{Th}$	$^{234}\text{U}/^{238}\text{U}$ (initial)	^{230}Th Age (yr) (uncorrected)	^{230}Th Age (yr BP)*** (corrected)
Se-09-6-(145mm)	NR	0.1649 \pm 0.0017	1.4566 \pm 0.0032	0.0009 \pm 0.0000	175.59	1.4737 \pm 0.0033	12987 \pm 137	12977 \pm 150
Se-09-6-(120mm)	345	0.1632 \pm 0.0031	1.4484 \pm 0.0077	0.0011 \pm 0.0000	152.25	1.4649 \pm 0.0080	12921 \pm 257	12857 \pm 295
Se-09-6-(103mm)	422	0.1503 \pm 0.0017	1.3911 \pm 0.0067	0.0009 \pm 0.0001	169.42	1.4050 \pm 0.0070	12373 \pm 144	12318 \pm 192
Se-09-6-(68mm)	369	0.1564 \pm 0.0021	1.4539 \pm 0.0062	0.0010 \pm 0.0000	157.92	1.4699 \pm 0.0064	12308 \pm 168	12246 \pm 214
Se-09-6-(11mm)	NR	0.1454 \pm 0.0013	1.4253 \pm 0.0028	0.0015 \pm 0.0001	94.60	1.4395 \pm 0.0028	11641 \pm 107	11583 \pm 123

Activity ratios were determined by MC-ICP-MS following Hellstrom (2003) (2). Ages in ka before present are corrected for initial ^{230}Th using eqn. 1 of Hellstrom (2006) (6), $(^{230}\text{Th}/^{232}\text{Th})_i$ of 0.9 ± 0.6 and the decay constants of Cheng et al (2013) (5). Uncertainties were propagated using Monte-Carlo simulation of each of the input activity ratios and initial ($^{234}\text{U}/^{238}\text{U}$) is calculated using the corrected age of each sample. U content is marked n.r. where sample weights were not recorded.

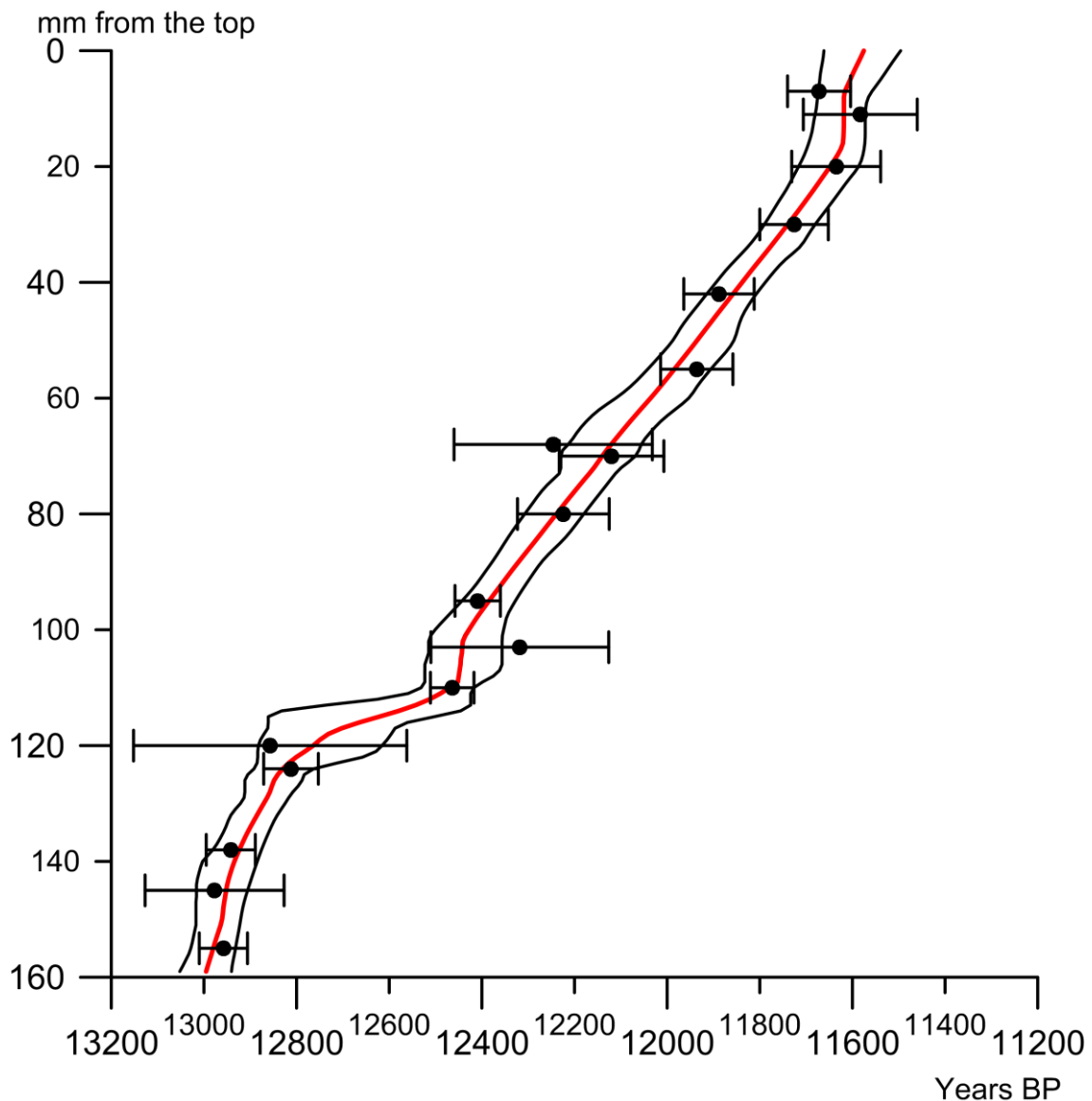


Figure S2. Age model of SE09-6 using StalAge software (7)

2. Supplementary Discussion

2.1. Interpretation of speleothem $\delta^{13}\text{C}$ and Mg/Ca data

SE09-6 $\delta^{13}\text{C}$ values show a variation of 3.37 ‰, from -5.40 ‰ to -8.77 ‰. The carbon isotopic variations may arise from both temperature-driven changes in the intensity of soil microbial activity and humidity-driven changes in the extent of degassing of drip waters. Thus, degassing due to pCO_2 cave air and prior calcite precipitation (8) are important processes that lead to higher $\delta^{13}\text{C}$ values during dry periods (9). Speleothem $\delta^{13}\text{C}$ values can also reflect changes in the dominant vegetation types (i.e. the C4/C3 plant ratio). However, changes in the ratio of C4/C3 plants are discarded here due to

absence of C4 plants in the Pyrenees today and in pollen records covering the Upper Pleistocene (10). Therefore, a more important factor influencing the $\delta^{13}\text{C}$ variability in the stalagmite may be plant root respiration and microbial activity of the soil and the epikarst zone. Carbon in speleothem calcite has two main sources: (1) soil CO_2 which is controlled by atmospheric CO_2 , plant respiration, and organic matter degradation; and (2) bedrock carbonate (CaCO_3) that is dissolved during seepage. In this way, in a dry period, soil activity and vegetation above the cave decrease and cause higher $\delta^{13}\text{C}$ values of soil CO_2 and, later on, enriched isotope values of speleothem carbonate (11, 12). Besides, during dry periods higher degrees of degassing accompany the slower drip rates and percolation through epikarst conduits and result in differential ^{12}C release and more positive $\delta^{13}\text{C}$ values in the precipitated calcite. Both processes shift $\delta^{13}\text{C}$ towards higher values; more positive $\delta^{13}\text{C}$ values in calcite are thus attributed to a drier climate. However, temperature also influences the amount of vegetation above the cave (13) since, in general, a warm climate will lead to a denser vegetation cover and, consequently, more negative $\delta^{13}\text{C}$ values in the stalagmite. Disentangling the effects of humidity and temperature requires information of the present-day cave system.

Present-day climate in the SCS area is characterized by two dry seasons (summer and winter) (Figure S3a) and ~73% of annual rainfall occurs during spring and fall. Higher temperatures are attained in summer (max. 32 °C) while minima of -4°C correspond to winter months. Due to this opposite influence of temperature and precipitation during the year, analyzing $\delta^{13}\text{C}$ and Mg/Ca in farmed calcite allows to better interpret those proxies in SE09-6 speleothem. During a 2-years period (2011 – 2012) $\delta^{13}\text{C}$ and Mg/Ca of calcite precipitated on glass slides located beneath ten active drips and collected at the end of every season were analysed. A significant seasonality, such as is observed in rainfall, is seen in the $\delta^{13}\text{C}$ and Mg/Ca data for every glass slide, with higher $\delta^{13}\text{C}$ values in summer and winter samples and lower values in spring and fall (Fig. S3b). Mg/Ca values follow the same pattern (Fig. S3c). Interannual variability is also evidenced with $\delta^{13}\text{C}$ mean/year values being lower in wet (e.g. 2011) than in dry years (e.g. 2012), revealing a clear response of $\delta^{13}\text{C}$ and Mg/Ca values to long-term variability in water availability. If temperature was the most important factor influencing the $\delta^{13}\text{C}$ values, winter and summer data won't be similar. Contrarily, both winter and summer $\delta^{13}\text{C}$ data plotted together associated to minimum rainfall (Fig. S3) demonstrating a clear influence of water availability. These data are then conclusive to interpret $\delta^{13}\text{C}$ and Mg/Ca values in SE09-6 as dry/wet conditions.

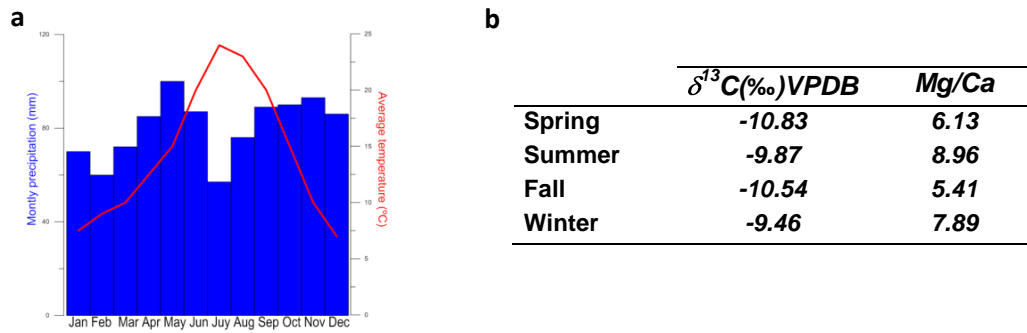


Figure S3. a, Climate diagram of the region where two dry (summer, winter) and wet (spring, fall) seasons are shown. b, Table with $\delta^{13}\text{C}$ and Mg/Ca values during the four monitored seasons (data averaged of the 10 glass slabs from years 2011 to 2013).

Besides those results from the monitoring survey, additional data based on U disequilibrium series are considered here in interpreting the $\delta^{13}\text{C}$ values (Fig. S4). Several studies have inferred drier conditions from higher values in the $^{234}\text{U}/^{238}\text{U}_0$ isotopic ratio based on the enrichment of ^{234}U related to the processes of α -recoil (14) and the consequent influence of rainfall, soil weathering and groundwater residence time (15). The fact that $\delta^{234}\text{U}$ values (Fig. S4) are stable throughout the Seso stalagmite record, suggests constant water-rock interaction processes and thus further supports the influence of precipitation-evaporation balance on $\delta^{13}\text{C}$ proxy as previously validated by the monitoring survey.

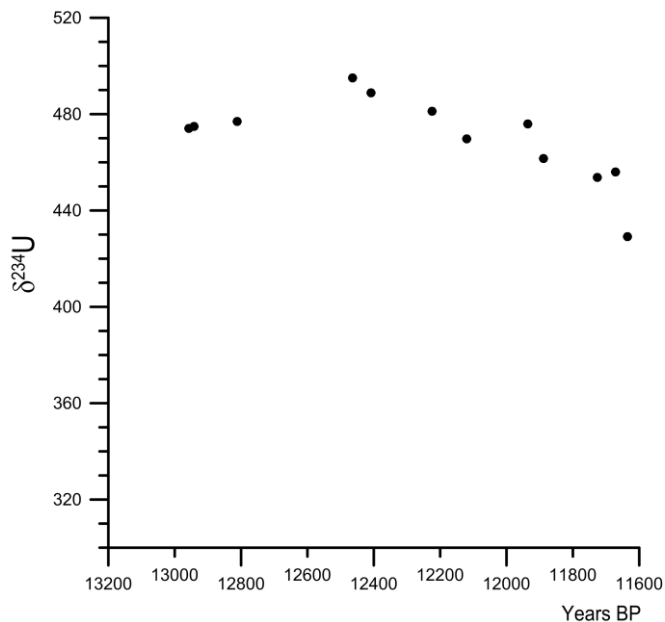


Figure S4. Variation of initial $\delta^{234}\text{U}$ content in SE09-6 speleothem through time

The Mg/Ca ratio is enhanced by slower drip rates but also by higher dripwater saturation states. These combined effects can be disentangled by comparing Mg/Ca with a second factor responsive to dripwater saturation state and drip interval, such as

the stalagmite growth rate, using kinetics of Dreybrodt et al (16), in the I-STAL model (17). We derived an inverse solution of variation in drip rate (drip interval, Fig. S5) using 30 s as minimum expected drip interval, 1 as the enrichment in Mg at maximum drip interval and 500 s as drip interval at maximum rock/soil exchange as main input parameters in I-STAL. These values may not represent precisely the dripwater parameters during stalagmite deposition, which are unknown, and therefore lead to some uncertainty in the absolute valued of model output for drip interval. However, the resulting temporal trends in drip interval are relatively insensitive to parameter selection within reasonable ranges (17) and therefore provide an estimate of temporal evolution in moisture balance. The lower driprates therefore suggest a shift to slightly drier conditions at the onset of GS-1 and no change until about 12,200 yr b2k.

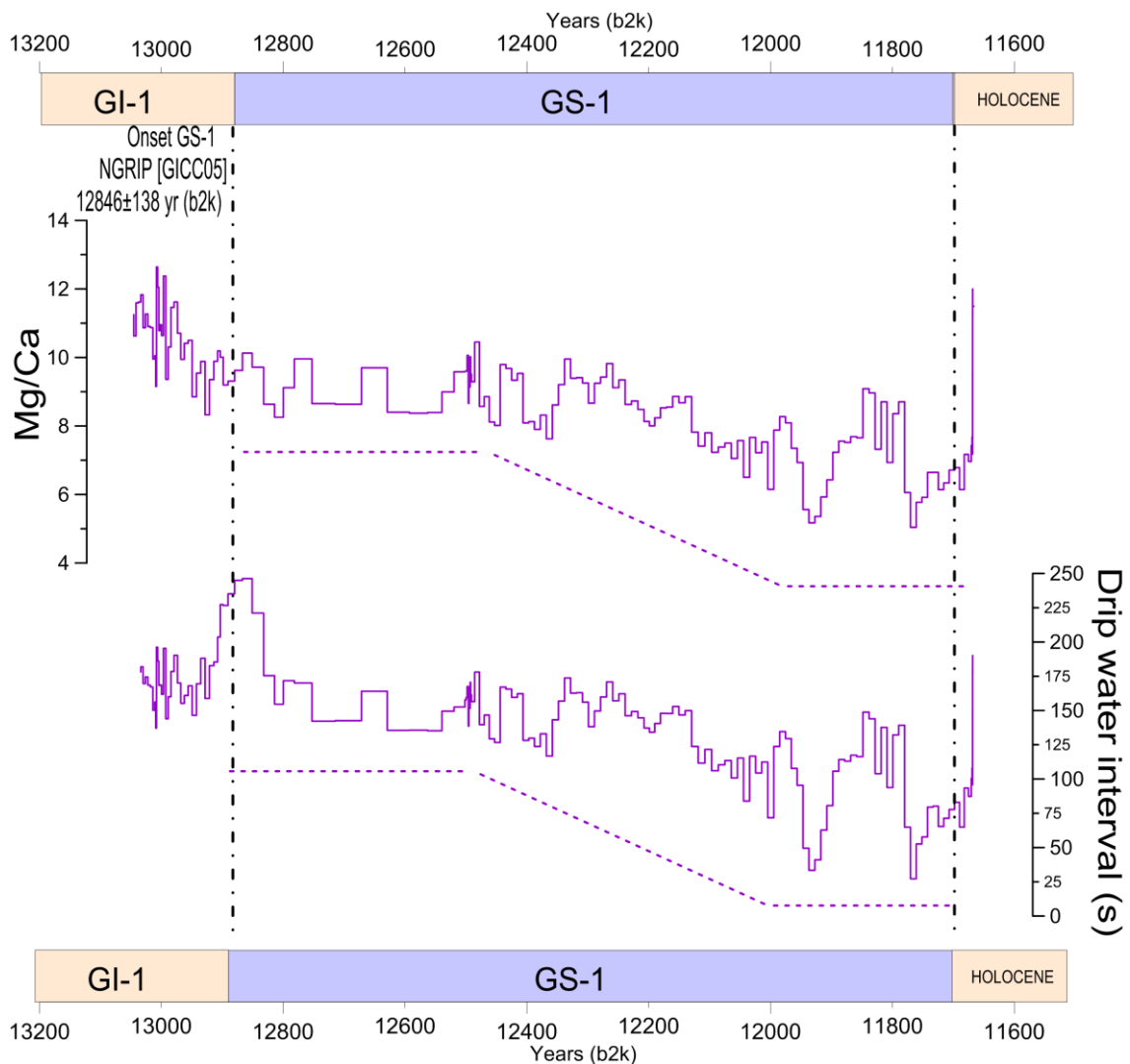


Figure S5. Mg/Ca profile and growth rate variation used to calculate drip rate using I-STAL(17).

2.2. Interpretation of speleothem $\delta^{18}\text{O}$ data

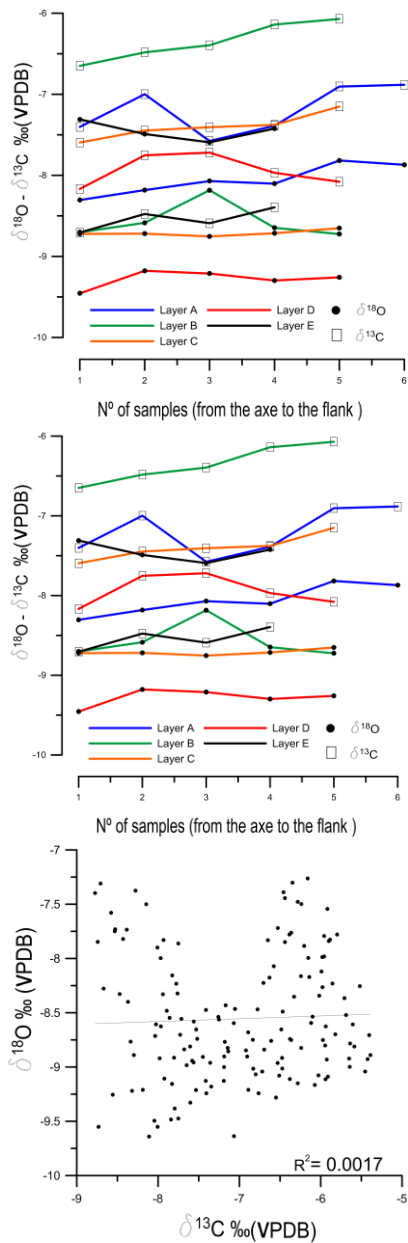


Figure S6. Hendy tests. From above to below, $\delta^{18}\text{O}$ (dots) and $\delta^{13}\text{C}$ (squares) variation along the five analysed layers. $\delta^{18}\text{O}$ vs $\delta^{13}\text{C}$ of all samples analysed along the growth axis. Spearman's rank correlation between $\delta^{18}\text{O}$ and $\delta^{13}\text{C}$ for each layer showing no significant correlation A: $R^2=0.54$, $p_{\text{value}}=0.242$. B: $R^2=-0.30$, $p_{\text{value}}=0.517$. C: $R^2=0.70$, $p_{\text{value}}=0.233$. D: $R^2=0.80$, $p_{\text{value}}=0.083$. E: $R^2=-0.20$, $p_{\text{value}}=0.750$.

Interpretation of $\delta^{18}\text{O}$ in speleothems ($\delta^{18}\text{O}_{\text{calcite}}$) requires the understanding of how different factors influence calcite values from rainfall to soil and epikarst variations (18). Thus, the $\delta^{18}\text{O}$ signal of speleothem calcite is affected by (i) the $\delta^{18}\text{O}$ value of the drip water feeding the stalagmite (19) and (ii) isotope fractionation processes occurring during calcite precipitation (20, 21). Replicating isotopic data is the best way to test the isotopic equilibrium in the cave (22). Unfortunately, replication of SE09-6 isotopic data has not been yet possible due to the lack of other stalagmites growing during GS-1 in the cave. We examined 16 additional samples from this cave but did not find a second stalagmite that grew during the YD. Only limited flowstone growth occurred during GS-1 but the samples are too thin to obtain a useful record. Thus, to test for isotope equilibrium of calcite precipitation in SE09-6 sample the correlation between $\delta^{13}\text{C}$ and $\delta^{18}\text{O}$ values was evaluated ($r^2=0.017$) and Hendy tests along five layers of the stalagmite (A, B, C, D and E) (Fig. S6) were made. Sampling along single layers was not easy due to the difficulty in following thin lamina. In general, a low correlation between the isotopic ratios and no $\delta^{18}\text{O}$ enrichment towards the flanks of the stalagmite is observed (Fig. S6). Although a weak correlation and some enrichment in ^{18}O towards the flanks is seen in layers A and D, this might be due to sampling inaccuracy. In essence, the data suggest that kinetic fractionation had only a minor effect and the measured calcite isotope values largely reflect climate (23).

At the Seso cave latitude, $\delta^{18}\text{O}$ values in precipitation ($\delta^{18}\text{O}_p$) are strongly linked to air temperature and probably less influenced by the amount of rainfall (“amount effect”) (24). Additionally, the altitude (eg. 0.15 to 0.5 ‰/100m of height) (25) and continentality (26) are further factors that modify the $\delta^{18}\text{O}_p$ values. A recent monitoring study carried out in Molinos cave (27) located in the Iberian Range in Northeast Spain indicates that event $\delta^{18}\text{O}_p$ values correlate significantly with air temperature ($r^2 = 0.33$; $p < 0.05$) and amount of precipitation ($r^2 = -0.19$; $p < 0.05$). Preliminary data from a nearby meteorological station in Seso cave area support this and indicate a preliminary temperature- $\delta^{18}\text{O}_p$ relationship of $0.47\text{‰}/^\circ\text{C}$ (larger than the $0.28\text{‰}/^\circ\text{C}$ measured in the Iberian Range). This influence of temperature on $\delta^{18}\text{O}_p$ is only partially compensated by the $-0.177\text{‰}/^\circ\text{C}$ due to calcite fractionation (20) thus allowing to contemplate using $\delta^{18}\text{O}_p$ in speleothems as temperature indicator in some areas from southern Europe. Fortunately, in Seso cave, the presence of actively-growing speleothems allows exploring the temperature - $\delta^{18}\text{O}_p$ relationship in more detail. MIC, a 7.5 cm-long stalagmite, was analysed for stable isotopes covering the last 200 years with a sampling resolution of 2.6 years (Fig S7, Table S2).

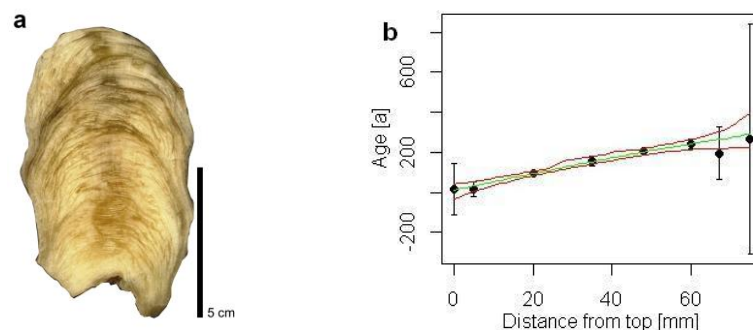


Figure S7. a, Image of MIC stalagmite. b, Age model (years AD) of MIC stalagmite using StalAge software (7) covering the last 200 years.

Table S2. MIC stalagmite ages from the University of Minnesota.

²³⁰ Th dating results. The error is 2σ error.									
Sample Number	²³⁸ U (ppb)	²³² Th (ppt)	²³⁰ Th / ²³² Th (atomic x10 ⁻⁶)	δ ²³⁴ U* (measured)	²³⁰ Th / ²³⁸ U (activity)	²³⁰ Th Age (yr) (uncorrected)	²³⁰ Th Age (yr 2011) (corrected)	δ ²³⁴ U _{initial} ** (corrected)	²³⁰ Th Age (yr BP)*** (corrected)
Mic-0	503.2 ±1.0	4623 ±93	4.8 ±0.2	485.9 ±2.4	0.0027 ±0.0001	196 ±6	16 ±128	485.9 ±2.4	-46 ±128
Mic-5	441.1 ±0.9	1166 ±23	5.8 ±1.0	487.3 ±2.3	0.0009 ±0.0002	69 ±11	17 ±38	487.3 ±2.3	-45 ±38
Mic-20	412.1 ±0.8	127 ±3	72.9 ±6.0	477.0 ±2.3	0.0014 ±0.0001	101 ±8	95 ±9	477.1 ±2.3	33 ±9
Mic-35	427.0 ±0.8	708 ±14	25.3 ±1.2	455.2 ±2.3	0.0025 ±0.0001	191 ±8	158 ±25	455.4 ±2.3	96 ±25
Mic-48	417 ±1	603 ±12	34 ±1	455.7 ±3.0	0.0030 ±0.0001	223 ±8	205 ±15	456 ±3	142 ±15
Mic-60	393 ±1	1049 ±21	23 ±1	461.4 ±3.8	0.0037 ±0.0001	274 ±8	242 ±24	462 ±4	179 ±24
Mic-67	413.4 ±0.9	3812 ±77	9.1 ±0.3	458.7 ±2.9	0.0051 ±0.0001	380 ±8	196 ±130	458.9 ±2.9	134 ±130
Mic-75	389 ±1	25715 ±517	3.6 ±0.1	458.0 ±2.5	0.0144 ±0.0002	1080 ±15	267 ±576	458 ±3	204 ±576

U decay constants: $\lambda_{238} = 1.55125 \times 10^{-10}$ (4) and $\lambda_{234} = 2.82206 \times 10^{-6}$ (5). Th decay constant: $\lambda_{230} = 9.1705 \times 10^{-6}$ (5).

* $\delta^{234}\text{U} = ([234\text{U}/238\text{U}]_{\text{activity}} - 1) \times 1000$. ** $\delta^{234}\text{U}_{\text{initial}}$ was calculated based on ^{230}Th age (T), i.e., $\delta^{234}\text{U}_{\text{initial}} = \delta^{234}\text{U}_{\text{measured}} \times e^{\lambda_{234}T}$. Corrected ^{230}Th ages assume the initial $^{230}\text{Th}/^{232}\text{Th}$ atomic ratio of $4.4 = 2.2 \times 10^{-6}$. Those are values for a material at secular equilibrium, with the bulk earth $^{232}\text{Th}/^{238}\text{U}$ of 3.8. The errors are arbitrarily assumed to be 50%.

***B.P stands for “Before Present” where “Present” is defined as the year 1950 A.D.

MIC $\delta^{18}\text{O}$ values vary between -7.71‰ and -6.37‰ with a marked increase since 1890 AD (red curve in Fig. S8). This pattern was replicated by two additional active speleothems from the same cave. Several instrumental temperature data of local to hemispheric coverage (28–30) and different paleotemperature reconstructions (31, 32) were used and compared with the $\delta^{18}\text{O}$ data of the MIC sample (Fig. S8). Visual inspection reveals a good match with all of them in the general patterns and an excellent correlation between NOAA data (Northern hemisphere land temperature anomaly) and MIC $\delta^{18}\text{O}$ data ($r^2=0.73$). This correlation suggests a value of $0.65\text{‰}/^\circ\text{C}$ for Late Holocene stalagmites from this region (Fig. S8). This influence of the temperature in stalagmite $\delta^{18}\text{O}$ values has been reported in other alpine caves, some of them located at similar altitude than Seso cave (33, 34). Therefore, the established correlation supports the use of $\delta^{18}\text{O}_c$ as a temperature proxy in SCS. Thus a temperature change of 1.3°C was calculated for the measured 2.14‰ range in the GS-1 stalagmite. This value is just a temperature estimation during GS-1 in this region since other factors may have changed during that time (eg. ocean water $\delta^{18}\text{O}$ value due to ice-volume changes or fresh-water pulses associated with meltwater events (35).

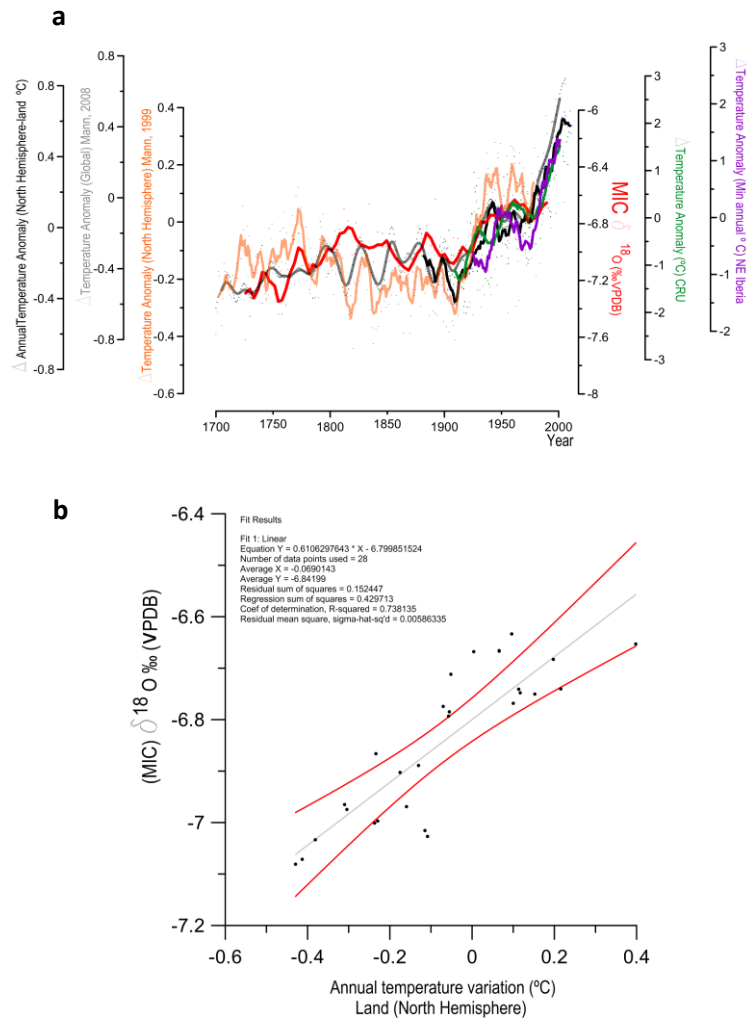


Figure S8. a, Comparison of $\delta^{18}O$ values of MIC stalagmite (red line, running average 10 yr) and instrumental temperature records taken from a compilation of stations from northeastern Spain (purple line) (28), NOAA and CRU Northern Hemisphere temperature data (black and green line) (29, 30) and two paleotemperature reconstructions (gray and orange lines) (31, 32). b, Correlation between $\delta^{18}O$ values in MIC stalagmite and Northern Hemisphere temperature land variation (30) ($r^2 = 0.73$).

Although less important than the temperature effect, the amount of precipitation is another factor controlling the variation of $\delta^{18}O$ as shown by carbonate precipitating on glass slides in Seso cave. In Fig. S9 the high similarity between external air temperature (gray curve) and carbonate $\delta^{18}O$ values is clearly shown but, additionally, the rainfall amount (blue curve) also exerts an influence on the isotopic composition of the carbonate. Thus, dry seasons, such as the winter of 2012, were characterized by higher $\delta^{18}O$ values than expected if only temperature was controlling isotope variability. The positive isotopic change (ca. 1 ‰) reflects a reduction of rainfall by 65% for that winter, superimposed on the temperature effect. Such an important change in precipitation amount in the past would be expected to produce a similar effect on $\delta^{18}O$ variability partly cancelling out the temperature effect.

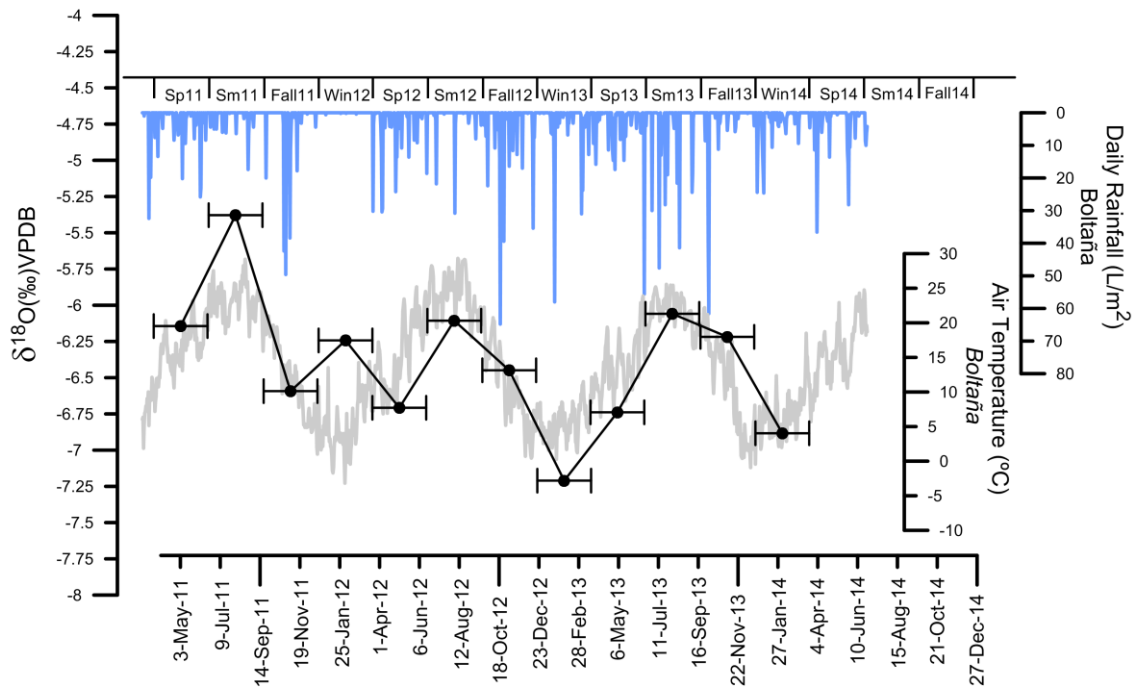


Figure S9. Three-year data of Seso cave monitoring showing external temperature and rainfall amount variation (obtained from a nearby meteorological station) compared to $\delta^{18}\text{O}$ variability measured on seasonally farmed calcite collected from glass slides.

References

1. Bartolomé M, et al. (2015) Upper Pleistocene interstratal piping-cave speleogenesis: The Seso Cave System (Central Pyrenees, Northern Spain). *Geomorphology* 228:335–344.
2. Hellstrom J (2003) Rapid and accurate U/Th dating using parallel ion-counting multi-collector ICP-MS. *Journal of Analytical Atomic Spectrometry* 18(11):1346–1351.
3. Cheng H, et al. (2000) The half-lives of uranium-234 and thorium-230. *Chemical Geology* 169:17–33.
4. Jaffey AH, Flynn KF, Glendenin LE, Bentley WC, Essling AM (1971) Precision Measurement of Half-Lives and Specific Activities of U235 and U238. *Phys Rev C* 4(5):1889–1906.
5. Cheng H, et al. (2013) Improvements in ^{230}Th dating, ^{230}Th and ^{234}U half-life values, and U–Th isotopic measurements by multi-collector inductively coupled plasma mass spectrometry. *Earth and Planetary Science Letters* 371-372:82–91.
6. Hellstrom J (2006) U–Th dating of speleothems with high initial ^{230}Th using stratigraphical constraint. *Quaternary Geochronology* 1(4):289–295.
7. Scholz D, Hoffmann DL (2011) StalAge - An algorithm designed for construction of speleothem age models. *Quaternary Geochronology* 6(3-4):369–382.

8. Matthey D, et al. (2008) A 53 year seasonally resolved oxygen and carbon isotope record from a modern Gibraltar speleothem: Reconstructed drip water and relationship to local precipitation. *Earth and Planetary Science Letters* 269(1-2):80–95.
9. Genty D, et al. (2003) Precise dating of Dansgaard-Oeschger climate oscillations in western Europe from stalagmite data. *Nature* 421:833–837.
10. González-Sampériz P, et al. (2006) Climate variability in the Spanish Pyrenees during the last 30,000 yr revealed by the El Portalet sequence. *Quaternary Research* 66(1):38–52.
11. Moreno A, et al. (2010) A speleothem record of rapid climatic shifts during last glacial period from Northern Iberian Peninsula. *Global and Planetary Change* 71:218–231; doi:10.1016/j.gloplacha.2009.10.002.
12. Genty D, et al. (2006) Timing and dynamics of the last deglaciation from European and North African $\delta^{13}\text{C}$ stalagmite profiles—comparison with Chinese and South Hemisphere stalagmites. *Quaternary Science Reviews* 25(17–18):2118–2142.
13. Martín-Chivelet J, Muñoz-García MB, Edwards RL, Turrero MJ, Ortega AI (2011) Land surface temperature changes in Northern Iberia since 4000 yr BP, based on $\delta^{13}\text{C}$ of speleothems. *Global and Planetary Change*. Available at: <http://linkinghub.elsevier.com/retrieve/pii/S0921818111000191>.
14. Hellstrom JC, McCulloch MT (2000) Multi-proxy constraints on the climatic significance of trace element records from a New Zealand speleothem. *Earth and Planetary Science Letters* 179(2):287–297.
15. Kaufman A, et al. (1998) U-Th isotope systematics from the Soreq cave, Israel and climatic correlations. *Earth and Planetary Science Letters* 156(3–4):141–155.
16. Dreybrodt W (1999) Chemical kinetics, speleothem growth and climate. *Boreas* 28(3):347–356.
17. Stoll HM, Müller W, Prieto M (2012) I-STAL, a model for interpretation of Mg/Ca, Sr/Ca and Ba/Ca variations in speleothems and its forward and inverse application on seasonal to millennial scales. *Geochemistry, Geophysics, Geosystems* 13(9):n/a–n/a.
18. Lachniet MS (2009) Climatic and environmental controls on speleothem oxygen-isotope values. *Quaternary Science Reviews* 28(5-6):412–432.
19. McDermott F (2004) Palaeo-climate reconstruction from stable isotope variations in speleothems: a review. *Quaternary Science Reviews* 23(7-8):901–918.
20. Tremaine DM, Froelich PN, Wang Y (2011) Speleothem calcite farmed in situ: Modern calibration of $\delta^{18}\text{O}$ and $\delta^{13}\text{C}$ paleoclimate proxies in a continuously-monitored natural cave system. *Geochimica et Cosmochimica Acta* 75(17):4929–4950.
21. Day CC, Henderson GM (2011) Oxygen isotopes in calcite grown under cave-analogue conditions. *Geochimica et Cosmochimica Acta* 75(14):3956–3972.
22. Dorale JA, Liu Z (2009) Limitations of Hendy test criteria in judging the paleoclimatic suitability of speleothems and the need for replication. *Journal of Cave and Karst Studies* 71(1):73–80.

23. Hendy CH (1971) The isotopic geochemistry of speleothems--I. The calculation of the effects of different modes of formation on the isotopic composition of speleothems and their applicability as palaeoclimatic indicators. *Geochimica et Cosmochimica Acta* 35(8):801–824.
24. Rozanski K, Araguás-Araguás L, Gonfiantini R (1993) Isotopic patterns in modern global precipitation. *Geophysical Monograph Series* 78:PP. 1–36.
25. Bowen GJ, Wilkinson B (2002) Spatial distribution of $\delta^{18}\text{O}$ in meteoric precipitation. *Geology* 30(4):315–318.
26. McDermott F, Atkinson TC, Fairchild IJ, Baldini LM, Matthey DP (2011) A first evaluation of the spatial gradients in $\delta^{18}\text{O}$ recorded by European Holocene speleothems. *Global and Planetary Change* 79(3–4):275–287.
27. Moreno A, et al. (2014) Climate controls on rainfall isotopes and their effects on cave drip water and speleothem growth: the case of Molinos cave (Teruel, NE Spain). *Clim Dyn* 43(1):221–241.
28. El Kenawy A, López-Moreno JI, Vicente-Serrano SM (2012) Trend and variability of surface air temperature in northeastern Spain (1920–2006): Linkage to atmospheric circulation. *Atmospheric Research* 106:159–180.
29. Brohan P, Kennedy JJ, Harris I, Tett SFB, Jones PD (2006) Uncertainty estimates in regional and global observed temperature changes: A new data set from 1850. *J Geophys Res* 111(D12):D12106.
30. Smith TM, Reynolds RW (2005) A Global Merged Land–Air–Sea Surface Temperature Reconstruction Based on Historical Observations (1880–1997). *J Climate* 18(12):2021–2036.
31. Mann ME, et al. (2008) Proxy-based reconstructions of hemispheric and global surface temperature variations over the past two millennia. *Proceedings of the National Academy of Sciences*.
32. Mann ME, Bradley RS, Hughes MK (1999) Northern hemisphere temperatures during the past millennium: Inferences, uncertainties, and limitations. *Geophys Res Lett* 26(6):759–762.
33. Mangini A, Spötl C, Verdes P (2005) Reconstruction of temperature in the Central Alps during the past 2000 yr from a $\delta^{18}\text{O}$ stalagmite record. *Earth and Planetary Science Letters* 235(3–4):741–751.
34. Boch R, et al. (2011) NALPS: a precisely dated European climate record 120–60 ka. *Clim Past Discuss* 7(2):1049–1072.
35. Broecker WS (2006) Was the Younger Dryas Triggered by a Flood? *Science* 312(5777):1146–1148.

Depth (mm from the top)	Age (yr b2k)	$\delta^{18}\text{O}$	$\delta^{13}\text{C}$	Mg/Ca
7	11666	-7.37	-8.28	11.49
8	11668	-7.82	-8.43	12
9	11668	-7.74	-8.39	11.38
10	11668	-7.75	-8.53	11.17
11	11668	-7.4	-8.77	9.59
12	11669	-7.85	-8.74	7.65
13	11669	-8.33	-8.47	7.18
14	11669	-7.31	-8.71	7.68
15	11669	-8.28	-8.67	7.43
16	11671	-7.73	-8.53	6.96
17	11675	-7.58	-8.58	7.17
18	11682	-7.5	-8.15	6.14
19	11690	-7.9	-8.01	6.78
20	11698	-7.83	-7.93	6.71
21	11707	-7.86	-7.75	6.34
22	11716	-8	-7.97	6.14
23	11725	-8.4	-8.37	6.65
24	11734	-8.23	-7.78	6.64
25	11743	-8.33	-7.94	5.92
26	11752	-8.55	-7.86	5.77
27	11761	-9.21	-8.19	5.04
28	11770	-9.22	-8.32	6.06
29	11780	-8.96	-7.36	8.7
30	11790	-8.91	-7.45	8.36
31	11799	-8.58	-7.56	6.93
32	11809	-8.54	-7.26	8.7
33	11819	-8.7	-7.73	7.32
34	11828	-8.81	-7.61	8.96
35	11838	-8.74	-7.52	9.09
36	11849	-8.94	-7.58	7.66
37	11859	-8.98	-7.65	7.69
38	11869	-8.91	-7.8	7.52
39	11878	-8.47	-7.41	7.56
40	11888	-8.96	-7.56	7.23
41	11898	-9.55	-8.01	6.43
42	11908	-9.64	-8.11	5.93
43	11918	-9.55	-8.73	5.36
44	11927	-9.26	-8.56	5.17
45	11937	-9.49	-8.04	5.56
46	11947	-9.47	-7.75	6.93
47	11957	-8.16	-7.82	7.35
48	11966	-8.32	-7.76	8.09
49	11976	-8.84	-7.68	8.27
50	11985	-8.48	-7.89	7.88
51	11995	-8.89	-8.3	6.15
52	12005	-8.71	-8.03	7.53
53	12015	-9.16	-7.83	7.22
54	12025	-8.56	-7.71	7.67
55	12035	-8.77	-8.34	6.5

56	12044	-8.63	-7.97	7.57
57	12054	-8.61	-8.03	7.05
58	12065	-8.92	-7.98	7.5
59	12075	-9.11	-7.92	7.39
60	12086	-9.24	-7.41	7.23
61	12097	-9.33	-7.6	7.8
62	12108	-9.38	-7.8	7.41
63	12119	-9.48	-7.84	7.82
64	12130	-9.18	-7.35	8.85
65	12140	-8.9	-7.19	8.68
66	12151	-8.86	-7.14	8.86
67	12161	-9.13	-7.19	8.55
68	12171	-8.77	-7.18	8.53
69	12181	-8.65	-7.53	8.24
70	12190	-8.56	-7.25	8
71	12199	-9.13	-7.41	8.13
72	12208	-9.21	-7.53	8.48
73	12218	-8.83	-7.14	8.73
74	12228	-8.43	-7.17	8.63
75	12239	-8.65	-6.49	9.34
76	12249	-8.47	-6.78	9.12
77	12259	-8.34	-6.02	9.82
78	12269	-9.11	-5.94	9.43
79	12279	-8.76	-6.61	9.25
80	12289	-9.08	-6.51	8.67
81	12299	-8.85	-6.92	9.25
82	12309	-8.68	-6.89	9.41
83	12319	-8.6	-7.07	9.39
84	12328	-9.02	-6.83	9.95
85	12338	-8.75	-6.36	9.21
86	12348	-9.04	-6.72	8.61
87	12358	-9.64	-7.07	7.63
88	12368	-9	-7.19	8.32
89	12378	-8.9	-6.9	7.9
90	12388	-9.24	-6.76	8.13
91	12397	-9.07	-6.8	8.09
92	12406	-8.49	-6.47	9.53
93	12416	-9.01	-6.47	9.34
94	12425	-9.16	-6.07	9.68
95	12434	-8.93	-5.92	9.79
96	12444	-8.92	-6.48	8.01
97	12453	-8.96	-6.53	8.12
98	12462	-8.84	-6.69	8.86
99	12470	-9.11	-6.38	8.57
100	12478	-8.26	-5.98	10.45
101	12486	-8.17	-6.14	9.29
102	12491	-8.74	-6.38	9.52
103	12492	-8.82	-6.24	10.02
104	12493	-9.21	-6.89	9.14
105	12495	-9.09	-5.91	8.66

106	12496	-8.52	-5.69	10.06
107	12498	-8.61	-5.61	9.61
108	12500	-8.93	-5.42	9.6
109	12502	-9	-5.64	9.58
110	12520	-9.15	-6.28	9
111	12540	-8.7	-5.82	8.39
112	12563	-9.08	-6.03	8.37
113	12593	-9.28	-6.55	8.4
114	12629	-8.37	-5.71	9.7
115	12672	-8.78	-5.64	8.63
116	12715	-8.89	-5.39	8.65
117	12753	-9.04	-5.45	9.96
118	12782	-8.75	-5.97	9.12
119	12800	-8.63	-5.94	8.26
120	12814	-8.71	-5.4	8.63
121	12832	-8.92	-5.65	9.72
122	12851	-8.59	-6.12	10.13
123	12867	-8.8	-5.94	9.62
124	12880	-8.23	-6.7	9.31
125	12891	-8.81	-5.59	9.2
126	12898	-8.54	-6.1	10.01
127	12903	-8	-6.15	10.19
128	12908	-7.85	-6.44	9.89
129	12914	-7.83	-6.65	9.35
130	12921	-8.35	-6.33	8.33
131	12928	-8.75	-6.83	9.88
132	12935	-8.47	-7.05	9.54
133	12942	-8.12	-5.99	8.85
134	12949	-8.23	-5.86	10.5
135	12956	-7.72	-6.53	10.41
136	12962	-7.44	-6.44	9.94
137	12968	-7.3	-6.35	10.71
138	12974	-7.79	-5.96	11.62
139	12979	-7.26	-6.16	11.46
140	12984	-7.78	-5.8	10.31
141	12989	-7.76	-6.36	9.36
142	12993	-8.26	-5.52	12.38
143	12997	-7.98	-5.96	10.64
144	13000	-7.48	-6.28	10.95
145	13002	-7.88	-6.2	10.78
146	13004	-7.54	-5.92	12.05
147	13006	-7.78	-6.38	12.64
148	13008	-7.39	-6.46	9.15
149	13009	-8.18	-6.63	10.05
150	13011	-7.99	-5.98	9.95
151	13014	-7.84	-5.9	10.87
152	13018	-7.83	-5.89	10.9
153	13022	-7.5	-6.24	11.27
154	13026	-8.07	-6.58	10.87
155	13030	-8.16	-6.24	11.83

156	13034	-7.78	-6.06	11.62
157	13038	-7.36	-5.79	11.59
158	13042	-7.59	-5.86	10.63
159	13045	-8.07	-6.21	11.25

Correction

EARTH, ATMOSPHERIC, AND PLANETARY SCIENCES

Correction for “Hydrological change in Southern Europe responding to increasing North Atlantic overturning during Greenland Stadial 1,” by Miguel Bartolomé, Ana Moreno, Carlos Sancho, Heather M. Stoll, Isabel Cacho, Christoph Spötl, Ánchel Belmonte, R. Lawrence Edwards, Hai Cheng, and John C. Hellstrom, which appeared in issue 21, May 26, 2015, of *Proc Natl Acad Sci USA* (112:6568–6572; first published May 11, 2015; 10.1073/pnas.1503990112).

The authors note that the affiliation for Isabel Cacho should instead appear as: Departament d'Estratigrafia, Paleontologia i Geociències Marines, Universitat de Barcelona, 28080 Barcelona, Spain. The authors also note that the affiliation for Christoph Spötl should instead appear as: Institut für Geologie, Universität Innsbruck, 6020 Innsbruck, Austria. The corrected author and affiliation lines appear below. The online version has been corrected.

Additionally, the authors note that the Acknowledgments section appeared incorrectly. It should instead appear as: “We thank the editor and two anonymous reviewers for several insightful comments that significantly improved the paper. This is a contribution to OPERA (CTM2013-48639-C2-2-RMEC), HIDROPAST (CGL2010-16376), CGL2009-10455/BTE, and CUEVAS PPNN (258/2011) projects funded by the Spanish Ministry of Economy and Competitiveness, the European Regional Development Fund, and the National Parks Autonomous Organism. The integrating ice core, marine and terrestrial records (INTIMATE) Cost Action (Cost-ES0907) is acknowledged for funding a research stay to M.B. at Innsbruck University.”

**Miguel Bartolomé^{a,b,1}, Ana Moreno^{a,c}, Carlos Sancho^b,
Heather M. Stoll^d, Isabel Cacho^e, Christoph Spötl^f,
Ánchel Belmonte^b, R. Lawrence Edwards^g, Hai Cheng^{g,h},
and John C. Hellstromⁱ**

^aInstituto Pirenaico de Ecología, Consejo Superior de Investigaciones Científicas, 50059 Zaragoza, Spain; ^bDepartamento de Ciencias de la Tierra, Universidad de Zaragoza, 50009 Zaragoza, Spain; ^cLaboratorio Internacional de Cambio Global, Pontificia Universidad Católica de Chile, Consejo Superior de Investigaciones Científicas, 8331150 Santiago, Chile; ^dDepartamento de Geología, Universidad de Oviedo, 33005 Oviedo, Spain; ^eDepartament d'Estratigrafia, Paleontologia i Geociències Marines, Universitat de Barcelona, 28080 Barcelona, Spain; ^fInstitut für Geologie, Universität Innsbruck, 6020 Innsbruck, Austria; ^gDepartment of Earth Sciences, University of Minnesota, Minneapolis, MN 55455; ^hInstitute of Global Environmental Change, Xian Jiaotong University, Xian 710049, China; and ⁱSchool of Earth Sciences, University of Melbourne, Melbourne, VIC 3010, Australia

www.pnas.org/cgi/doi/10.1073/pnas.1510485112